



City Research Online

City, University of London Institutional Repository

Citation: Weygandt, M., Hummel, H-M., Schregel, K., Ritter, K., Allefeld, C., Dommès, E., Huppke, P., Haynes, J. D., Wuerfel, J. & Gärtner, J. (2017). MRI-based diagnostic biomarkers for early onset pediatric multiple sclerosis. *NeuroImage: Clinical*, 7, pp. 400-408. doi: 10.1016/j.nicl.2014.06.015

This is the published version of the paper.

This version of the publication may differ from the final published version.

Permanent repository link: <https://openaccess.city.ac.uk/id/eprint/22802/>

Link to published version: <https://doi.org/10.1016/j.nicl.2014.06.015>

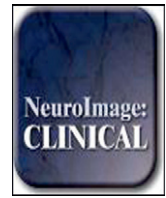
Copyright: City Research Online aims to make research outputs of City, University of London available to a wider audience. Copyright and Moral Rights remain with the author(s) and/or copyright holders. URLs from City Research Online may be freely distributed and linked to.

Reuse: Copies of full items can be used for personal research or study, educational, or not-for-profit purposes without prior permission or charge. Provided that the authors, title and full bibliographic details are credited, a hyperlink and/or URL is given for the original metadata page and the content is not changed in any way.

City Research Online:

<http://openaccess.city.ac.uk/>

publications@city.ac.uk



MRI-based diagnostic biomarkers for early onset pediatric multiple sclerosis



Martin Weygandt^{a,b,1,*}, Hannah-Maria Hummel^{c,1}, Katharina Schregel^d, Kerstin Ritter^{a,b}, Carsten Allefeld^a, Esther Dommès^e, Peter Huppke^c, John-Dylan Haynes^{a,b,2}, Jens Wuerfel^{b,d,2,**}, Jutta Gärtner^{c,2}

^aBernstein Center for Computational Neuroscience Berlin, Charité – Universitätsmedizin, Berlin, Germany

^bNeuroCure Clinical Research Center, Charité – Universitätsmedizin Berlin, Germany

^cDepartment of Pediatrics and Pediatric Neurology, and German Center for Multiple Sclerosis in Childhood and Adolescence, University Medicine Göttingen, Germany

^dInstitute of Neuroradiology, University Medicine Göttingen, Germany

^eCenter for Internal Medicine and Dermatology, Department of Psychosomatic Medicine, Charité – Universitätsmedizin Berlin, Germany

ARTICLE INFO

Article history:

Received 24 March 2014

Received in revised form 17 June 2014

Accepted 30 June 2014

Available online 12 July 2014

Keywords:

Pediatric multiple sclerosis

Early onset pediatric multiple sclerosis

Biomarkers

Diagnostic information

ABSTRACT

Currently, it is unclear whether pediatric multiple sclerosis (PMS) is a pathoetiologically homogeneous disease phenotype due to clinical and epidemiological differences between early and late onset PMS (EOPMS and LOPMS). Consequently, the question was raised whether diagnostic guidelines need to be complemented by specific EOPMS markers. To search for such markers, we analyzed cerebral MRI images acquired with standard protocols using computer-based classification techniques. Specifically, we applied classification algorithms to gray (GM) and white matter (WM) tissue probability parameters of small brain regions derived from T2-weighted MRI images of EOPMS patients (onset <12 years), LOPMS patients (onset ≥12 years), and healthy controls (HC). This was done for PMS subgroups matched for disease duration and participant age independently. As expected, maximal diagnostic information for distinguishing PMS patients and HC was found in a periventricular WM area containing lesions (87.1% accuracy, $p < 2.2 \times 10^{-5}$). MRI-based biomarkers specific for EOPMS were identified in prefrontal cortex. Specifically, a coordinate in middle frontal gyrus contained maximal diagnostic information (77.3%, $p = 1.8 \times 10^{-4}$). Taken together, we were able to identify biomarkers reflecting pathognomonic processes specific for MS patients with very early onset. Especially GM involvement in the separation between PMS subgroups suggests that conventional MRI contains a richer set of diagnostically informative features than previously assumed.

© 2014 The Authors. Published by Elsevier Inc. This is an open access article under the CC BY-NC-ND license (<http://creativecommons.org/licenses/by-nc-nd/3.0/>).

1. Introduction

Pediatric MS (PMS) is defined by an initiation prior to the age of 16 years (Sadaka et al., 2012; Renoux et al., 2007). Although a variety of features characteristic for PMS have been described recently (e.g., Hummel et al., 2013; Bigi and Banwell, 2012; Sadaka et al., 2012; Vargas-Lowy et al., 2012; Polman et al., 2011), it is currently unclear whether PMS denotes a pathoetiologically homogeneous or heterogeneous clinical phenotype. In particular, recent studies found evidence for differences in the gender distribution between patients with early onset PMS (EOPMS) as compared to later onset PMS (LOPMS; Banwell

et al., 2007). Another study evaluated the validity of the revised McDonald criteria 2010 for diagnosing PMS and found that these criteria are well suited for children with onset at the age of 11 or older, but considerably less well for the subgroup of children with earlier onset (Sadaka et al., 2012). Comparing characteristics of hyperintense lesions in T2-weighted (T2w) brain MR images between EOPMS and LOPMS patients, Chabas and colleagues found that EOPMS lesions were less well-defined. Consistently, these authors claimed that MRI-based diagnostic criteria for prepubertal MS might have to be revised (Chabas et al., 2008).

In recent years, the application of computer-based classification algorithms for the analysis of MRI data of neurological (e.g., Kloepfel et al., 2008) as well as psychiatric disorders (e.g., Weygandt et al., 2012) has become more and more frequent. In MS research, a variety of neuroimaging studies used this approach to identify lesion-related and non-lesion-related MRI biomarkers for adult MS extracted from brain images acquired with clinical routine MRI acquisition protocols. For example, we applied this approach to diagnose relapsing–remitting MS (RRMS) by evaluating voxel intensity patterns (Weygandt et al.,

* Correspondence to: M.Weygandt, Bernstein Center for Computational Neuroscience, Charité – Universitätsmedizin Berlin, Haus 6, Philippstrasse 13, 10115 Berlin, Germany.

** Correspondence to: J. Würfel, Institute of Interventional and Diagnostic Neuroradiology, University Medicine Göttingen, Robert-Koch-Str. 40, 37075 Göttingen, Germany. Tel.: +49 (0) 551 396643, Fax: +49 (0) 551 3913250

E-mail address: martin.weygandt@bccn-berlin.de (M. Weygandt).

¹ First authors contributed equally to this work.

² Last authors contributed equally to this work.

2011), and wavelet representations of these patterns (Hackmack et al., 2012a) extracted from brain areas containing normal-appearing brain tissue measured with T2w MRI sequences. In a further study, we used tissue intensity patterns to predict symptom severity in RRMS (Hackmack et al., 2012b). Finally, another group used the approach to differentiate between subgroups of MS (i.e. patients with short vs. long disease duration; high vs. low white matter (WM) lesion load; benign vs. non-benign MS) based on gray matter (GM) probability maps (Bendfeldt et al., 2012).

In the present study, we assessed whether classification techniques can also be applied in pediatric neuroimaging by searching for MRI-based diagnostic biomarkers specific for EOPMS. In particular, we conducted three main diagnostic classification analyses to identify brain regions containing the most relevant diagnostic information for EOPMS. In Analysis 1, we investigated differential diagnostic separability of EOPMS vs. LOPMS patients using logistic regression. This was done independently for areas located in GM and for areas located in WM based on local tissue probability parameters. In Analysis 2, we searched for diagnostic information for separation of EOPMS patients vs. healthy control (HC) subjects separately for GM and WM areas. Finally, in Analysis 3 we tested local diagnostic separability of LOPMS vs. HC based on local GM and WM tissue probability parameters. Importantly, LOPMS and HC were matched with EOPMS with regard to gender, the LOPMS and EOPMS group were additionally matched in terms of disease duration and lesion load. In three supplementary analyses, the same comparisons were additionally computed for PMS subgroups matched for age, gender and lesion load.

2. Methods and materials

2.1. Participants

Participants were included in the study in a three-step procedure. In the first step, 79 MS patients with a disease onset prior to the age of 16 years and 20 HC subjects scanned with a standardized MR protocol (see [Brain imaging](#)) were included. All pediatric MS patients were diagnosed according to the revised McDonald diagnostic criteria 2010 (Polman et al., 2011). Each patient was followed-up at the German National Center for Multiple Sclerosis in Childhood and Adolescence, University Medical Center, Göttingen, Germany. HC subjects were free of neurological or psychiatric disorders. Compatible with the heuristic for age-based patient subdivision presented in Ruggieri et al. (2004), patients with disease onset prior to the age of twelve were assigned to the EOPMS group, and patients with onset at 12 years or older were assigned to the LOPMS group. In the second step, we (MW) conducted an MRI quality assessment procedure leading to exclusion of the data of eight EOPMS patients, 20 LOPMS patients, and five healthy participants (primarily due to slight motion artifacts). Finally, the six EOPMS patients with the longest and the 14 LOPMS patients with the shortest disease duration were excluded in the third step in order to match the two groups in terms of disease duration. Following these steps, 15 patients with EOPMS, 16 patients with LOPMS, and 15 HC subjects were finally included. For the supplementary analyses, two alternative PMS groups were composed to match these groups in terms of participant age. Specifically, the five youngest EOPMS patients and the 13 oldest LOPMS patients were excluded. Thus, 16 patients with EOPMS, 17 patients with LOPMS, and 15 HC subjects were included in these supplementary analyses. Consent was obtained according to the Declaration of Helsinki, and the local research ethics committee of the Medical Faculty, Georg-August University, Göttingen approved the study. All subjects gave written informed consent.

2.2. Brain imaging

Whole-brain high in-plane resolution T2w images with 32 or 35 contiguous axial slices (TR = 4500 ms, TE = 103 ms, flip angle =

130°, voxel resolution = $0.6 \times 0.6 \times 4 \text{ mm}^3$, no gap, matrix size = 384×384) were acquired with a turbo spin echo sequence on a 3 Tesla whole-body MRI (Magnetom Trio, Siemens, Erlangen, Germany) using a clinical routine 12-channel head coil. In particular, in the three main analyses evaluating PMS groups matched for disease duration (in the three supplementary analyses evaluating PMS groups matched for participant age) images of 2 (2) EOPMS patients had 32 axial slices, images of 13 (14) had 35 slices. For LOPMS patients, 9 (4) had 32 and 7 (13) had 35 slices, 3 (3) HC subjects had 32, 12 (12) HC subjects 35 slices. A χ^2 -test for stochastic independence showed that the number of slices acquired was partly balanced across groups i.e. EOPMS vs. LOPMS: $\chi^2 = 6.23$, $p = 0.013$ ($\chi^2 = 0.67$, $p = 0.412$), EOPMS vs. HC: $\chi^2 = 0.24$, $p = 0.624$ ($\chi^2 = 0.32$, $p = 0.570$), and LOPMS vs. HC $\chi^2 = 4.29$, $p = 0.038$ ($\chi^2 = 0.06$, $p = 0.810$).

2.3. Preprocessing of MRI data

Preprocessing included a manual lesion mapping procedure, two sequential segmentation runs, resampling and within-subject standardization of modulated tissue probability maps. In particular, we (HH) started preprocessing by performing a manual lesion mapping based on high in-plane resolution T2w-images (voxel size = $0.6 \times 0.6 \times 4 \text{ mm}^3$) of individual subjects using the OsiriX software toolbox (OsiriX Foundation, Geneva, Switzerland).

Subsequently, images were segmented into GM, WM and CSF in a two-run segmentation procedure using the unified segmentation approach in SPM8 (Wellcome Trust Centre for Neuroimaging, Institute of Neurology, UCL, London, UK – <http://www.fil.ion.ucl.ac.uk/spm>). The two-run procedure was applied to minimize age-dependent deformation effects (e.g., Wilke et al., 2002) and tissue misclassification (e.g., Wilke et al., 2003) that might result in a typical one-run procedure from using adult reference data during normalization/segmentation of pediatric brain images.

In the first segmentation run, the standard adult tissue probability templates included in SPM8 were used. Regions containing lesions identified by HH were excluded. Unmodulated tissue probability maps and spatially normalized lesion masks were generated as output files for each subject. These output files were then used to compute customized tissue probability templates for the second segmentation run separately for each pair of groups (EOPMS & LOPMS, EOPMS & HC and LOPMS & HC) and for both matching procedures. In particular, customized tissue probability templates were determined by computing the voxel-wise averages across not modulated tissue probability maps for GM, WM and CSF of each subject included in the given pair of groups. To avoid lesion-induced artifacts, subjects having a lesion at a given voxel coordinate (as defined by the normalized lesion masks) were excluded from the averaging procedure.

In the second segmentation run, these customized tissue probability templates for GM, WM, and CSF were used (please note that the images of the EOPMS and LOPMS patients were segmented twice within each matching framework: once for the comparison with the HC subjects, once for the comparison with the other PMS group). Again, regions containing lesions were excluded. Modulated and unmodulated tissue probability maps and spatially normalized lesion maps were generated as output files for each subject. After segmentation, the modulated probability maps were resampled to a voxel resolution of $6 \times 6 \times 6 \text{ mm}^3$ using trilinear interpolation to increase sensitivity of the diagnostic classification analyses and to decrease the substantial computational load imposed by the voxel-wise permutation procedure used for statistical inference (please see section MRI-based classification analyses).

In the next step, unmodulated probability maps were used to generate binary masks for GM, WM, and CSF. This was done for each pair of groups and matching framework separately to facilitate a tissue-specific search for diagnostic biomarkers in the classification analyses. Specifically, we first computed the voxel-wise average for each of the three tissue types across unmodulated tissue probability maps (voxel resolution =

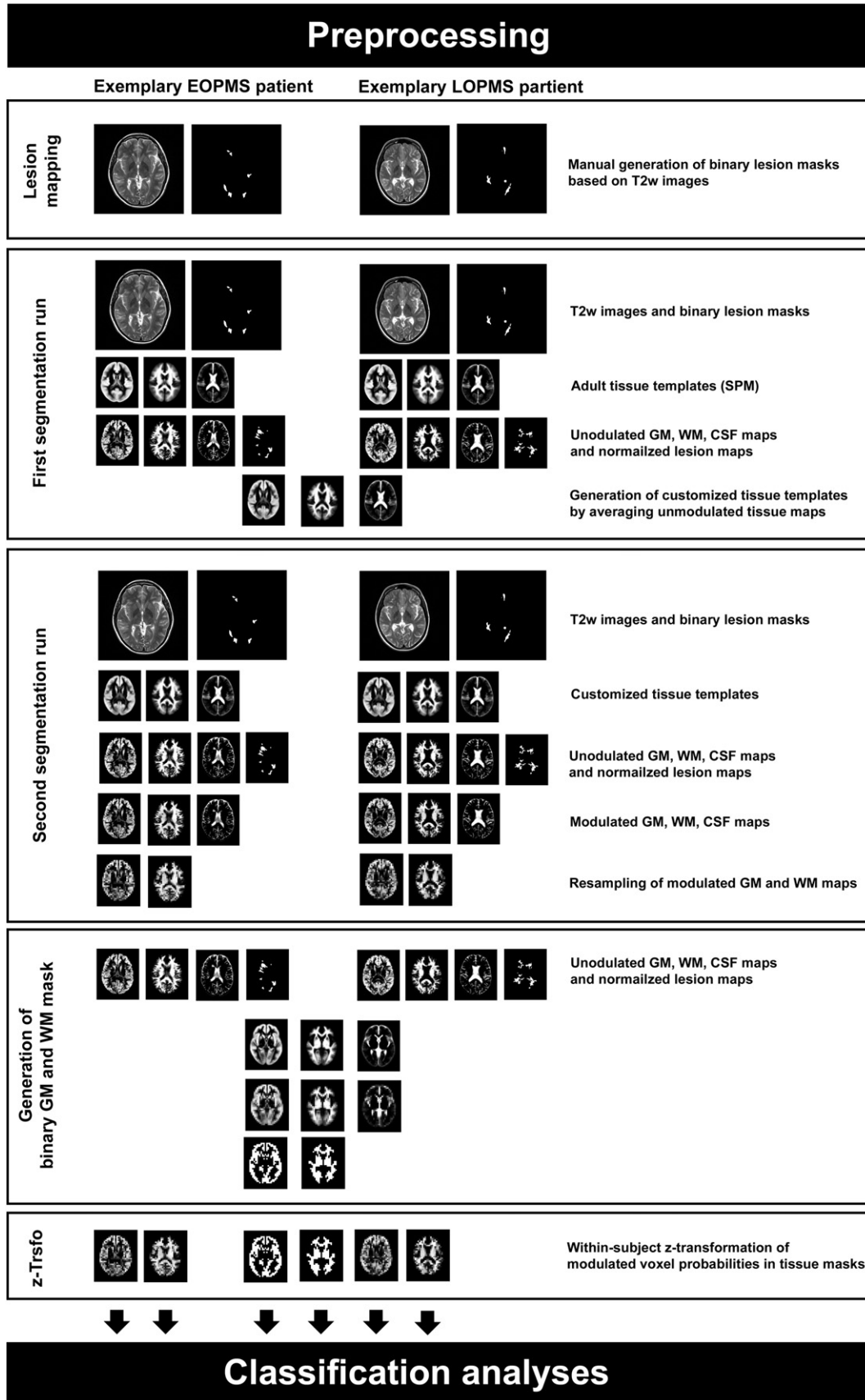


Fig. 1. Preprocessing of MRI data. Starting with the second segmentation run, preprocessing was performed separately for each of the pairs of groups. The figure shows two exemplary subjects belonging to the early onset PMS vs. later onset PMS pair. EOPMS, early onset pediatric MS; LOPMS, later onset pediatric MS; T2w, T2-weighted; z-Trsfo, z-transformation.

Table 1

Demographic and clinical characteristics for pediatric MS groups matched for gender and disease duration. Lesion load was computed based on lesion masks manually determined by HH derived from on high-resolution T2w-images in the lesion mapping procedure. Clinical symptoms were diagnosed by an experienced neuropediatrician and a medical consultant. Abbreviations: Dis. dur., disease duration; s., symptoms; Unspec., unspecified, Cran. nrv. involv., cranial nerve involvement.

Demographic and clinical participant characteristics									
Parameter	EOPMS	LOPMS	HC	EOPMS vs. LOPMS		EOPMS vs. HC		LOPMS vs. HC	
	M (SD)	M (SD)	M (SD)	<i>t</i>	<i>p</i>	<i>t</i>	<i>p</i>	<i>t</i>	<i>p</i>
Age (years)	11.9 (2.7)	16.4 (1.4)	12.6 (2.7)	-5.85	2.3×10^{-6}	-0.74	0.466	5.00	2.7×10^{-5}
Onset (years)	8.5 (2.3)	14.0 (1.2)		-8.46	2.5×10^{-9}				
Dis. dur. (mo)	40.6 (24.4)	28.9 (13.0)		1.67	0.105				
Lesion load ($\times 10^4$ mm ³)	2.2 (4.4)	2.4 (3.0)		-0.14	0.886				
	N (total = 15)	N (total = 16)	N (total = 15)	χ^2	<i>p</i>	χ^2	<i>p</i>	χ^2	<i>p</i>
Gender (female)	9	13	12	1.70	0.193	1.43	0.232	0.01	0.930
Motor s.	7	1		6.61	0.010				
Visual s.	5	6		0.06	0.809				
Sensible s.	5	8		0.88	0.347				
Unspec. s.	6	2		3.06	0.080				
Cran. nrv. involv.	2	0		2.28	0.131				

$2 \times 2 \times 2$ mm³) of all subjects included in a given pair of groups that did not have a lesion at a given coordinate. Whether a lesion was present for a given coordinate or not was determined based on the normalized lesion masks determined in the second segmentation run. Then, we resampled these averaged maps to a voxel resolution of $6 \times 6 \times 6$ mm³. Finally, a voxel coordinate was assigned to that tissue class for which the maximal averaged probability score among the three tissues was computed. Following this procedure, the GM mask comprised 4498 (supplementary analysis using age-matched samples: 4641) voxels for the contrast EOPMS vs. LOPMS, the WM mask for this comparison comprised 2379 (2513) voxels. For EOPMS vs. HC, the GM mask consisted of 5015 (4951) voxels, the mask for WM consisted of 2186 (2301) voxels. Finally, for LOPMS vs. HC the GM mask consisted of 4632 (4727) voxels, the mask for WM consisted of 2519 (2510) voxels.

In a final step, we computed a within-subject z-transformation of the masked, resampled, and modulated GM and WM tissue probability maps for each subject to account for potential between group differences of overall brain volume. The resulting z-transformed, masked, resampled and modulated tissue probability maps then entered the classification analyses (see below). Please see Fig. 1 for an overview on preprocessing steps conducted.

Table 2

Gray and white matter brain areas with diagnostic information for the separation of early onset pediatric MS (EOPMS) and later onset pediatric MS (LOPMS) patients. Area, GM region of the closest brain region of a given coordinate as determined by the neuroanatomical atlas of the Montreal Neurological Institute (MNI) brain template (Tzourio-Mazoyer et al., 2002). H, Hemisphere; Dst, Euclidean distance to the closest brain region contained in the neuroanatomical atlas in millimeters. Please note, that a distance of 0 mm in the white matter analysis might result from the comparably liberal assignment of coordinates to GM in the MNI atlas. *x*, *y*, *z*, *x*, *y*, and *z* coordinates of the identified coordinate in MNI space in millimeters. RMSE, root mean square error; *p*, probability of observed RMSE according to permutation testing. MSS, mean of sensitivity and specificity. SEN, sensitivity; SPE, specificity; Δtp , mean difference of standardized and modulated tissue probability between both groups. Ls, percentage of patients having a lesion at a given coordinate. Bold text indicates a diagnostic accuracy on a significance level corrected for multiple comparisons (false discovery rate [FDR] criterion; $\alpha_{FDR} = 0.05$). Non-bold text indicates a diagnostic accuracy according to an uncorrected significance threshold ($\alpha_{uncorrected} = 5 \times 10^{-4}$). Brain area abbreviations: Ant., anterior; cing., cingulate; front., frontal, gy., gyrus; Inf., inferior; ncl. nucleus. Mid, middle; par., parietal; op., operculum; Postcent., postcentral; Sup., superior; temp., temporal.

GM areas with diagnostic information for EOPMS vs. LOPMS												
Area	H	Dst	<i>x</i>	<i>y</i>	<i>z</i>	RMSE	<i>p</i>	MSS	SEN	SPE	Δtp	Ls
Rolandic op.	R	0	48	-12	18	0.41	1.2×10^{-4}	74.2	73.3	75.0	0.9	0
Inf. front. gy.	L	0	-36	30	-20	0.42	1.8×10^{-4}	77.3	73.3	81.3	0.9	0
Mid. temp. gy.	R	0	54	-48	12	0.42	2.0×10^{-4}	87.3	93.3	81.3	0.8	0
Mid. front. gy.	R	0	24	32	-18	0.42	3.2×10^{-4}	80.6	80.0	81.3	1.0	0
Inf. par. gy.	R	0	48	-36	54	0.43	4.7×10^{-4}	70.8	66.7	75.0	-1.3	0
WM areas with diagnostic information for EOPMS vs. LOPMS												
Area	H	Dst	<i>x</i>	<i>y</i>	<i>z</i>	RMSE	<i>p</i>	MSS	SEN	SPE	Δtp	Ls
Angular gy.	R	3.6	36	-58	24	0.35	$< 2.1 \times 10^{-5}$	80.6	80.0	81.3	-1.6	10
Pallidum	L	0	-24	-6	0	0.40	3.6×10^{-5}	80.8	86.7	75.0	0.7	0
Sup. front. gy.	L	0	-18	54	12	0.43	2.9×10^{-4}	74.2	73.3	75.0	0.3	10
Insula	L	1.0	-36	-30	24	0.43	4.1×10^{-4}	67.7	66.7	68.8	-1.1	13
Sup. front. gy.	L	1.0	-18	54	0	0.42	4.5×10^{-4}	67.9	73.3	62.5	0.3	3

2.4. MRI-based classification analyses

We conducted three separate main analyses to discover diagnostic information that potentially differentiates EOPMS, LOPMS and HC. In particular, we searched for diagnostic information for separation of EOPMS vs. LOPMS patients contained in modulated tissue probability parameters extracted from GM (WM) areas in classification Analysis 1a (1b). In classification Analysis 2a (2b), we searched for diagnostic information for EOPMS patients vs. HC subjects in GM (WM) areas. Finally, in Analysis 3a (3b), we searched for diagnostic information for separation of LOPMS patients vs. HC subjects based on GM (WM) tissue parameters. In these main analyses, PMS groups were matched with regard to disease duration, lesion load and age. In three supplementary analyses (S1–S3) the same comparisons were computed for PMS subgroups matched for gender, age and lesion load. The processing steps did not differ between analyses, except for group- and tissue-specific brain masks and the tissue-specific modulated probability maps used for the analyses (see Preprocessing). The classification analyses were conducted using in-house software (cf. Weygandt et al., 2012; Weygandt et al., 2011).

For each voxel, we determined the diagnostic classification accuracy in a leave-one-out cross-validation (CV) framework. In particular, we

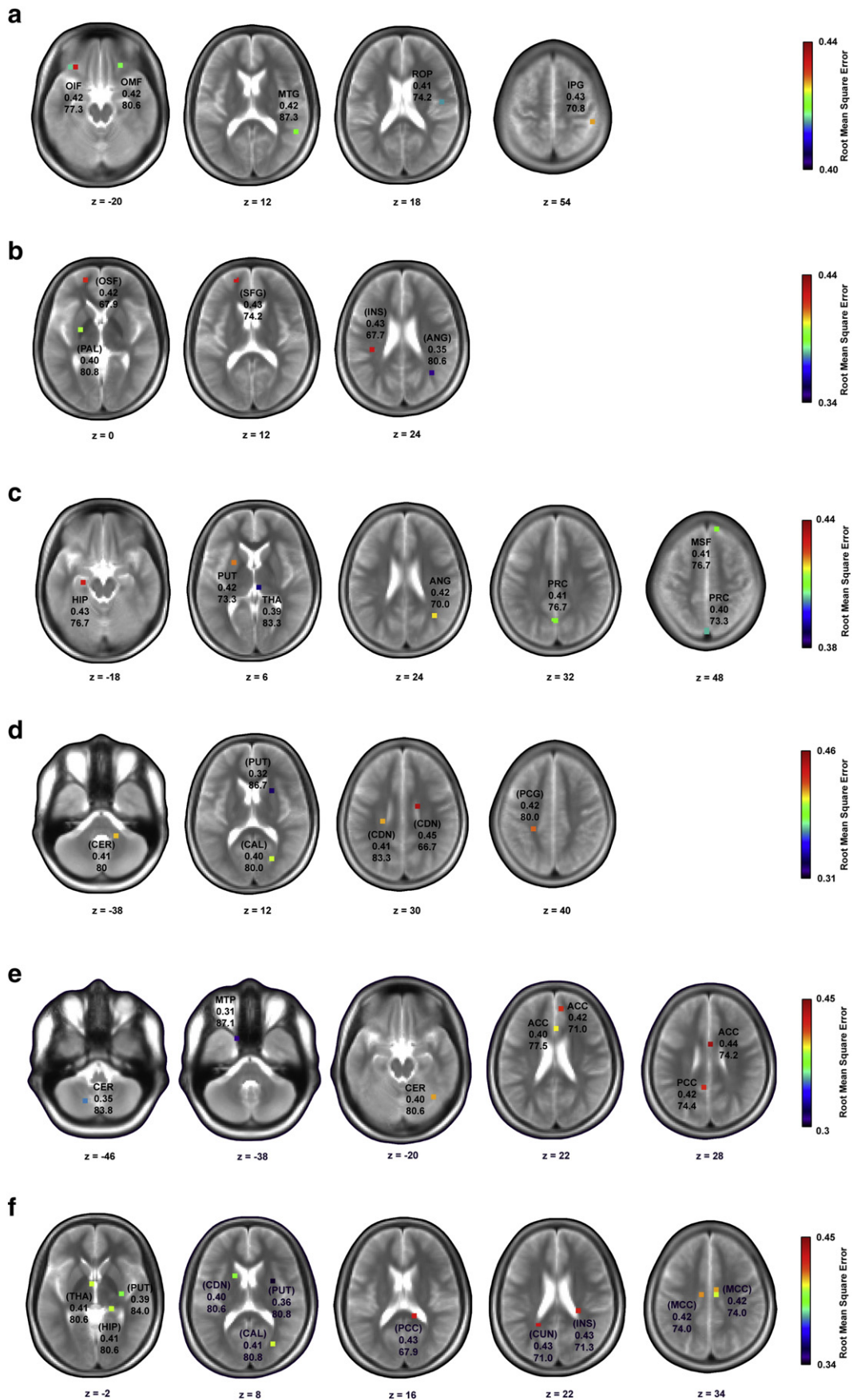


Table 3

Gray and white matter brain areas with diagnostic information for the separation of early onset pediatric MS (EOPMS) patients and healthy controls (HC). See Table 2 for details. Brain area abbreviations: cing., cingulate; fiss., fissure; gy., gyrus; ncl. nucleus. par., parietal; Postcent., postcentral; Sup., superior.

GM areas with diagnostic information for EOPMS vs. HC												
Area	H	Dst	x	y	z	RMSE	p	MSS	SEN	SPE	Δtp	Ls
Precuneus	L	0	0	-76	50	0.40	7.2×10^{-5}	73.3	80.0	66.7	0.4	0
Angular gy.	R	3.6	36	-58	24	0.42	1.1×10^{-4}	70.0	80.0	60.0	1.3	7
Thalamus	R	0	6	-24	6	0.39	2.5×10^{-4}	83.3	86.7	80.0	-0.5	0
Precuneus	L	0	0	-64	32	0.41	2.5×10^{-4}	76.7	73.3	80.0	-0.9	0
Putamen	L	0	-24	6	6	0.42	2.9×10^{-4}	73.3	66.7	80.0	-0.7	0
Hippocampus	L	0	-24	-18	-18	0.43	3.4×10^{-4}	76.7	80.0	73.3	0.6	7
Sup. front. gy.	R	0	12	46	48	0.41	4.9×10^{-4}	76.7	66.7	86.7	-1.3	0
WM areas with diagnostic information for EOPMS vs. HC												
Area	H	Dst	x	y	z	RMSE	p	MSS	SEN	SPE	Δtp	Ls
Putamen	R	0	24	12	12	0.32	$< 2.3 \times 10^{-5}$	86.7	86.7	86.7	0.7	0
Calcarine fiss.	R	0	24	-70	14	0.40	1.0×10^{-4}	80.0	73.3	86.7	-0.9	20
Postcent. gy.	L	4.4	-24	-34	40	0.42	1.8×10^{-4}	80.0	80.0	80.0	-0.3	27
Caudate ncl.	L	7.2	-24	-24	30	0.41	2.7×10^{-4}	83.3	80.0	86.7	-0.5	27
Caudate ncl.	R	4	18	-6	30	0.45	2.7×10^{-4}	66.7	66.7	66.7	-0.8	27
Cerebellum	R	2.2	18	-42	-38	0.41	3.6×10^{-4}	80.0	80.0	80.0	0.5	0

started the analysis by extracting the modulated tissue probability score (from either the modulated GM or WM probability map) of each subject included in the analysis (N_{total}) for a given voxel (e.g., for the comparison EOPMS vs. LOPMS in the disease duration matching framework: $N_{\text{total}} = 15[N_{\text{EOPMS}}] + 16[N_{\text{LOPMS}}] = 31$). Then, the data of all but one subject ($N_{\text{total}} - 1$) were used as training data to compute a logistic regression model using the GLMFIT function included in Matlab 7.6 (The MathWorks Inc., Natick, MA, 2008). In the next step, this model was used to compute the predicted class membership probability of the left out or test subject respectively based on its modulated tissue probability score. This procedure was repeated N_{total} times i.e. until each subject included in the analysis was once excluded from building the regression model/once treated as test subject.

In the next step, we computed the root mean square error (RMSE) between true class labels (EOPMS vs. LOPMS: EOPMS = 1, LOPMS = 0; EOPMS vs. HC: EOPMS = 1, HC = 0; LOPMS vs. HC: LOPMS = 1, HC = 0) and predicted class membership probabilities as primary diagnostic accuracy measure for each voxel coordinate. As secondary/illustrative accuracy measure, we computed the mean of sensitivity and specificity (MSS). For that measure, a correctly classified subject belonging to the group named first in each comparison (e.g., an EOPMS patient in the comparison 'EOPMS vs. LOPMS') was considered as true positive, a correctly classified subject belonging to the second group (LOPMS in the example) was considered as true negative, etc. The diagnostic classification procedure was repeated for each voxel coordinate included in the respective analysis and yielded a diagnostic accuracy map for that analysis which denoted the RMSE (MSS) score for each voxel.

To test for significance of diagnostic accuracy obtained for each voxel, we used permutation testing to compute the probability of the observed RMSE-score under the null hypothesis. The False Discovery Rate (FDR; Benjamini and Hochberg, 1995) criterion was used to correct for multiple comparisons. Following the FDR criterion, the number of permutations necessary to assess the significance of accuracy in each

voxel equals the number of tests (i.e. voxels) included in each analyses divided by the false positive rate for a single test ($\alpha_{\text{single test}} = 0.05$). Thus, for example in Analysis 1a we permuted the class labels of each voxel 4498 (number of voxels in GM mask for EOPMS vs. LOPMS) / 0.05 ($\alpha_{\text{single test}} = 0.05$) = 89,960 times. Then, we used the resulting permutation distribution of RMSE-scores for each voxel to assess the significance of the observed RMSE-score under the null hypothesis (Good et al., 2005). At this point, we would like to mention that due to the direct link between number of voxels in an analysis on one hand and the number of tests per analysis and the number of permutations necessary per test on the other permutation testing might easily involve a massive computational burden – if the number of voxels is very high. For that reason, we decided to resample the voxel resolution during image preprocessing in order to decrease the computational load.

In the Results section, we report coordinates for which RMSE is significant on a threshold corrected for multiple comparisons following the FDR criterion ($\alpha_{\text{FDR}} = 0.05$) and also voxel coordinates significant according to an uncorrected threshold ($\alpha_{\text{uncorrected}} = 5 \times 10^{-4}$). Results reported correspond to coordinates in the anatomical standard space of the MNI-brain template (Tzourio-Mazoyer et al., 2002). Since the classification analyses were conducted in customized template space, it was necessary to map the coordinates identified in the analyses to MNI-space first. The procedure used for this mapping is described in the Supplementary methods.

3. Results

3.1. Demographic and clinical participant characteristics

LOPMS patients and HC subjects did not differ from EOPMS patients with regard to gender (EOPMS vs. LOPMS: $\chi^2 = 1.70$, $p = 0.193$; EOPMS vs. HC: $\chi^2 = 1.43$, $p = 0.232$). Following from the disease duration matching procedure, the average age in the LOPMS group was

Fig. 2. Brain areas with diagnostic information. Gray matter (GM) areas with significant diagnostic information for the separation of a) early onset pediatric MS (EOPMS) and late onset pediatric MS (LOPMS) patients. c) EOPMS and healthy control (HC) subjects, e) LOPMS and HC. White matter (WM) areas with diagnostic information for the separation of b) EOPMS and LOPMS patients, d) EOPMS and HC, and f) LOPMS and HC. Significant coordinates are shown superimposed on subjects' mean T2-weighted MRI image co-registered to the standard space of the Montreal Neurological Institute (MNI) brain template (Tzourio-Mazoyer et al., 2002). In panels a, c, and e, brain area abbreviations refer to the GM region a given coordinate is located in as determined by the MNI brain atlas (Tzourio-Mazoyer et al., 2002). In panels b, d, and f, brain area abbreviations in brackets refer to the GM region with the closest Euclidean distance to a given WM coordinate as determined by the MNI brain atlas. As accuracy measure, we computed the root mean square error (RMSE) between class labels and predicted class membership probability and denoted it beneath area abbreviations. For illustrative purposes, we also report the mean of sensitivity and specificity (MSS) as alternative accuracy measure beneath RMSE scores. Indices beneath axial brain slices report the z-coordinate in MNI space. Slices are displayed in neurological orientation. Brain area abbreviations: ACC, anterior cingulate cortex; ANG, angular gyrus; CAL, calcarine fissure; CDN, caudate nucleus; CER, cerebellum; CUN, cuneus; HIP, hippocampus; INS, insular cortex; IPG, inferior parietal gyrus; MCC, middle cingulate gyrus; MSF, medial superior frontal gyrus; MTG, middle temporal gyrus; OIF, orbital inferior frontal gyrus; OMF, orbital middle frontal gyrus; OSF, orbital superior frontal gyrus; PAL, pallidum; PCC, posterior cingulate gyrus; PCG, postcentral gyrus; PRC, precuneus; PUT, putamen; ROP, rolandic operculum; SFG, superior frontal gyrus; THA, thalamus.

significantly higher than in the EOPMS group (EOPMS vs. LOPMS: $t = -5.9$, $p = 2.3 \times 10^{-6}$). In addition, the average age in the LOPMS group was also higher as in the HC group (LOPMS vs. HC: $t = 5.0$, $p = 2.7 \times 10^{-5}$). A t -test for independent samples revealed that both PMS subgroups were comparable in terms of T2w lesion volume ($t = -0.14$, $p = 0.886$). See [Table 1](#) for further details. Please see [Table S1](#) for participant characteristics of PMS subgroups matched by age and gender.

3.2. Analysis 1: diagnosing EOPMS vs. LOPMS

In this analysis, we searched for differential diagnostic information for separation of EOPMS vs. LOPMS patients contained in modulated tissue probability parameters extracted from GM (WM) areas in classification Analysis 1a (1b). Analysis 1a primarily revealed frontal and parietal GM areas as being diagnostically informative. Consistently, WM Analysis 1b revealed diagnostic information in WM areas located in the vicinity of frontal gyri. Please see [Table 2](#) and [Fig. 2a and b](#) for details. Please see [Table S2](#) for results for this group comparison based on PMS subgroups matched for age, gender and lesion load.

3.3. Analysis 2: diagnosing EOPMS vs. HC

In classification Analysis 2a (2b), we searched for diagnostic features separating between EOPMS patients and HC subjects contained in modulated tissue probability parameters extracted from GM (WM) areas. In Analysis 2a, a number of GM areas in vicinity of the lateral ventricles have been identified. However, consistent with Analysis 1, also a coordinate in superior frontal gyrus was found. Analysis 2b revealed WM coordinates close to the striatum, cerebellum but also postcentral gyrus and calcarine fissure. Please see [Table 3](#) and [Fig. 2c and d](#) for details. Please see [Table S3](#) for results regarding this group comparison based on EOPMS patients that were matched to LOPMS patients in terms of age, gender and lesion load.

3.4. Analysis 3: diagnosing LOPMS vs. HC

Finally, in Analysis 3a (3b) we searched for GM (WM) areas containing diagnostic information for the separation of LOPMS patients and HC subjects. Consistent with the difference in the presence of disease and the difference in mean participant age between the groups, Analyses 3a and b revealed a comparatively large number of coordinates with significant diagnostic information. Please see [Table 4](#) and [Fig. 2e and f](#) for details. Notably, contrary to Analysis 1 and 2, no frontal or orbitofrontal gyri or WM coordinates in the vicinity of these areas were identified. Please see [Table S4](#) for results regarding this group comparison based on LOPMS patients that were matched to EOPMS patients in terms of age, gender and lesion load.

4. Discussion

In this study, we identified diagnostic features in conventional MRI images separating between EOPMS patients, LOPMS patients and HC subjects by applying computer-based classification techniques to locally specific brain tissue probability information.

Three main analyses were conducted that investigated diagnostic separability within the three pairs of groups (EOPMS vs. LOPMS, EOPMS vs. HC, and LOPMS vs. HC) based on gray as well as white matter voxel tissue probability information. In these analyses, the PMS groups were matched by disease duration, lesion load and gender whereas the same comparisons were computed in three supplementary analyses (S1 – S3) based on PMS groups matched for age, lesion load and gender.

Consistent with the literature (e.g., [Zivadinov et al., 2013](#); [Polman et al., 2011](#); [Morgen et al., 2006](#); [Prinster et al., 2006](#); [Filippi and Rocca, 2005](#)), a set of widely distributed brain areas was identified across analyses. Among these, areas were detected that are discussed

as key markers for MS such as WM areas in vicinity of e.g. caudate nucleus and thalamus (i.e. 'periventricular' WM areas, cf. [Polman et al., 2011](#)) and for these areas, very high accuracy has been obtained. Specifically, for the separation of EOPMS and HC (based on PMS groups matched for age, gender and lesion load, Analysis S2), an accuracy of 87.1% has been reached for a WM coordinate close to caudate nucleus (MNI: -18, -18, 30). However, besides these well established markers temporal and frontal GM areas have also been identified, which are less well known to be diagnostically relevant, although their general involvement in MS has repeatedly been reported (e.g., [Morgen et al., 2006](#); [Prinster et al., 2006](#)). For example, 87.1% accuracy has been reached for a GM locus in the middle temporal pole (MNI: -16, 10, -38) for the separation of LOPMS and HC (based on PMS groups matched for disease duration, gender and lesion load, Analysis 3).

Unfortunately, identification of biomarkers for the separation of EOPMS patients from HC subjects or even for EOPMS vs. LOPMS patients alone does not necessarily imply that the markers are also specific for EOPMS. To the contrary, many of the markers found for EOPMS vs. HC are considered to be generic markers for MS. Markers found for EOPMS vs. LOPMS are not necessarily specific as PMS subgroups differed in terms of age in Analysis 1 (or disease duration in Analysis S1). These differences cannot be easily avoided by e.g. another matching procedure because they follow from the conjunction of a) the mutual dependence of the factors disease onset, disease duration and age (e.g., age is the sum of disease onset and duration) and b) the definition of EOPMS and LOPMS in terms of their different disease onset, disease duration and age (e.g., age is the sum of disease onset and duration) and b) the definition of EOPMS and LOPMS in terms of their different disease onset. Thus, within this constellation, balancing one of the factors disease duration or age automatically results in inducing a bias in the other.

Consequently, balancing alone cannot be sufficient to guarantee specificity of biomarkers identified in the comparison EOPMS vs. LOPMS. Instead, an additional group comparison must be taken into account that is comparably characterized by a difference in age or disease duration. Specifically, given that certain findings are made only in the EOPMS vs. LOPMS comparison but not for a pair of groups that is similarly characterized by one of these confounding factors, it is unlikely that underlying differences observed in EOPMS vs. LOPMS are induced by the confound since its effect should be comparable across analyses.

A comparison for which this condition was fulfilled was LOPMS vs. HC (Analysis 3). In particular, the average age in the LOPMS group was higher than in the EOPMS group and (comparably) higher than in the HC group (see [Table 1](#)). Consequently, biomarkers identified in the EOPMS vs. LOPMS but not in the LOPMS vs. HC comparison should not depend on differences in participant age (and disease duration) and should thus be specific for EOPMS. This specific result pattern was found for frontal gyri and WM areas located in the vicinity to frontal GM gyri. In particular, Analysis 1 identified a coordinate in middle ([MNI: 24, 32, -18], MSS = 80.6%) and inferior frontal gyri ([MNI: -36, 30, -20], 77.3% MSS) with diagnostic information. In addition, a WM area in vicinity to superior frontal gyrus ([MNI: -18, 54, 12], MSS = 74.2%) also contained diagnostic information. On the contrary, frontal gyri were not at all identified in Analysis 3 and Analysis S3. Thus, taken together the integration of findings made across analyses conducted in the study suggest that disease-related alterations of frontal gyri starting early after disease onset is a diagnostically relevant feature specific for EOPMS.

Besides identifying brain MRI-based biomarkers specific for EOPMS, the study also demonstrates that computer-based classification approaches are able to utilize subtle tissue variations for diagnosis, extracted from GM but also WM that are less characterized by pronounced intensity alterations than hyperintense WM lesions in T2w-images. This was revealed by the GM analyses conducted as most of the coordinates with diagnostic information did not contain lesions (see [Tables 2–4](#) and [S1–S3](#)). Non-lesion GM based separation of EOPMS and HC is in line with findings of studies showing GM loss in adult MS patients compared to HC

Table 4

Gray and white matter brain areas with diagnostic information for the separation of late onset pediatric MS (LOPMS) patients and healthy controls: HC see Table 2 for details. Brain area abbreviations: Ant., anterior; cing., cingulate; gy., gyrus; Inf., inferior; ncl. nucleus. Mid, middle; par., parietal; Op., operculum; Parahipp., parahippocampal; Post., posterior; Postcent., postcentral; Sup., superior; temp., temporal.

GM areas with diagnostic information for LOPMS vs. HC												
Area	H	Dst	x	y	z	RMSE	p	MSS	SEN	SPE	Δtp	Ls
Mid. temp. pole	L	0	-16	10	-38	0.31	< 1.1 × 10⁻⁵	87.1	87.5	86.7	0.5	0
Cerebellum	L	0	-16	-66	-46	0.35	2.7 × 10⁻⁵	83.8	87.5	80.0	1.0	0
Ant. cing. gy.	L	0	2	22	22	0.40	4.3 × 10⁻⁵	77.5	75.0	80.0	0.9	0
Cerebellum	R	0	38	-60	-20	0.40	1.6 × 10 ⁻⁴	80.6	81.3	80.0	0.5	0
Parahipp. gy.	R	6.1	14	4	-32	0.41	1.9 × 10 ⁻⁴	74.2	75.0	73.3	0.7	0
Post. cing. gy.	L	0	-6	-48	28	0.42	2.0 × 10 ⁻⁴	74.4	68.8	80.0	-0.6	0
Sup. temp. gy.	L	0	-52	-2	-8	0.40	2.3 × 10 ⁻⁴	80.6	81.3	80.0	1.0	0
Ant. cing. gy.	R	0	8	46	22	0.42	2.5 × 10 ⁻⁴	71.0	68.8	73.3	-1.0	0
Ant. cing. gy.	R	1	2	4	28	0.44	3.2 × 10 ⁻⁴	74.2	75.0	73.3	0.9	0
Cerebellum	L	0	-10	-44	-28	0.42	4.0 × 10 ⁻⁴	74.2	75.0	73.3	0.4	0
WM areas with diagnostic information for LOPMS vs. HC												
Area	H	Dst	x	y	z	RMSE	p	MSS	SEN	SPE	Δtp	Ls
Putamen	R	0	26	0	8	0.35	< 2.0 × 10⁻⁵	80.8	75.0	86.7	0.7	0.0
Thalamus	R	0	14	-26	4	0.36	4.6 × 10 ⁻⁵	84.0	81.3	86.7	1.0	0.0
Calcarine fiss.	R	0	26	-72	10	0.41	4.7 × 10 ⁻⁵	80.8	75.0	86.7	-0.9	37.5
Putamen	R	0	32	-14	-2	0.39	4.9 × 10 ⁻⁵	84.0	81.3	86.7	0.8	6.3
Caudate ncl.	L	1	-16	10	10	0.40	9.3 × 10 ⁻⁵	80.6	81.3	80.0	0.7	6.3
Mid. cing. gy.	R	0	8	-10	34	0.42	9.3 × 10 ⁻⁵	74.0	81.3	66.7	0.8	12.5
Putamen	L	0	-28	4	4	0.40	1.2 × 10 ⁻⁴	77.5	75.0	80.0	0.8	0.0
Gy. rectus	R	2	14	28	-8	0.42	2.0 × 10 ⁻⁴	81.0	68.8	93.3	-0.7	6.3
Insula	R	9.2	26	-32	22	0.43	2.6 × 10 ⁻⁴	71.3	62.5	80.0	-0.7	37.5
Cuneus	L	6.3	-22	-48	26	0.43	2.7 × 10 ⁻⁴	71.0	68.8	73.3	-0.9	62.5
Mid. cing. gy.	L	1.0	-10	-14	34	0.42	2.8 × 10 ⁻⁴	74.0	81.3	66.7	1.0	6.3
Post. cing. gy.	R	1.4	14	-38	16	0.43	3.1 × 10 ⁻⁴	67.9	62.5	73.3	-1.1	12.5
Hippocampus	R	0	20	-32	-2	0.41	3.3 × 10 ⁻⁴	80.6	81.3	80.0	-1.0	0.0
Thalamus	L	3.0	-4	-2	-2	0.41	3.6 × 10 ⁻⁴	80.6	81.3	80.0	-0.7	0.0
Thalamus	L	0	-16	-28	4	0.44	3.7 × 10 ⁻⁴	67.5	75.0	60.0	0.6	0.0

(Weygandt et al., 2011; Ceccarelli et al., 2009; Morgen et al., 2006; Prinster et al., 2006; Bakshi et al., 2002). Within these studies (i.e. Ceccarelli et al., 2009; Bakshi et al., 2002), it was assumed that elevated iron deposition might lead to tissue loss in deep gray matter nuclei which in turn induces signal hypointensity in T2w-images. Speculatively, this mechanism might also underly GM-based separability of PMS groups and HC.

Interestingly, utilization of non-lesion related MRI signals for the diagnosis of EOPMS vs. HC by the regression approach in addition to utilization of lesion-related signals was also supported by white matter analyses. In particular, although high diagnostic accuracy was frequently linked to high lesion occurrence in these analyses – what is in line with the diagnostic guidelines (Polman et al., 2011) implying that lesions are the only MRI features indicative of MS – high lesion occurrence alone was frequently not sufficient to explain accuracy obtained by the regression approach. This can be seen e.g. in Analysis 2b for a WM coordinate (MNI: -24, -34, 40) located in the vicinity of postcentral gyrus. Although a substantial proportion of EOPMS patients had a lesion at this coordinate (i.e. 4 out of 15 or 26.7%, see Table 3) accuracy expectable by this lesion occurrence was lower than accuracy obtained by the logistic regression approach. Specifically, when following the diagnostic guidelines (Polman et al., 2011) suggesting that lesions are the only MRI alterations indicative of MS, and when additionally assuming that lesions do only occur in patients but not controls, this lesion occurrence should go along with a diagnostic accuracy of 63.4%. In particular, given that four out of 15 patients, who should present with lesions, had a lesion at this coordinate (sensitivity = 26.7%), and none of 15 controls, who should not have lesions, had a lesion (specificity = 100%), a mean of sensitivity and specificity of 63.4% follows. Contrary to these 63.4% however, the logistic regression approach evaluating continuous tissue probability parameters (instead of the dichotomously scaled 'presence of a lesion' marker evaluated by human raters) obtained 80.0% mean of sensitivity and specificity. Consequently, the discrepancy between these accuracies suggests that the regression approach utilizes

further MRI signals in addition to lesion-induced signal alterations. Speculatively, WM characterized by only slight signal hyperintensities being too weak to be classified as lesion by a human rater (i.e. so-called 'dirty-appearing' white matter; Ge et al., 2003) might be these signals. This interpretation would be compatible with our recent findings (Weygandt et al., 2011).

At first glance, the moderate sample sizes of groups investigated might be considered a drawback of the study. However, within the specific framework of the present study several aspects have to be considered when evaluating the sample size. First, we were able to identify diagnostic information in periventricular WM areas containing lesions. Periventricular WM lesions are considered (one of) the key diagnostic marker(s) for MS (e.g., Polman et al., 2011). Thus, the sample size was sufficient to reliably identify this major MRI marker for MS frequently reported in the literature. Second, from a pragmatic perspective the small prevalence of pediatric MS has to be considered. Following Ruggieri et al. (2004), the prevalence of MS with an onset prior to the age of 16 years is approximately between 0.003% and 0.006% in the overall population. For MS with an onset prior to the age of 10 years it is even less – approximately between 0.0002% and 0.0008%. Thus, EOPMS and even LOPMS are rare clinically cases. Finally, we used non-parametric permutation testing to estimate the probability of diagnostic accuracies obtained on the voxel level. Compared with parametric procedures, permutation tests rely much less on the fulfillment of distributional assumptions for a given test statistic (Good, 2005) – a problem that might be more prominent in moderately sized data sets as compared to larger data sets.

Finally, the small deviations in the number of slices acquired for T2w-images across groups for PMS groups matched with regard to disease duration, lesion load and gender might be considered as limitation of the study. However, the impact of this imbalance does not appear to be very strong since results obtained for Analyses 1–3 are compatible with those obtained in Analyses S1–S3. And for the latter analyses the number of slices was balanced across groups.

5. Conclusion

In this study, we identified diagnostic features in MRI acquired during clinical routine that differentiated between EOPMS patients, LOPMS patients and HC subjects by applying computer-based classification techniques to locally specific brain tissue probability information. In particular, we were able to replicate existing knowledge on the pivotal role of hyperintense WM lesions for MS diagnosis by using this approach to the separate between PMS patients and HC subjects. By using the classification approach for differential diagnosis or separation of PMS subgroups respectively, we found diagnostic information specific for EOPMS in frontal gyri and also WM areas in the vicinity of frontal gyri. These results suggest that conventional MRI contains a richer set of diagnostically informative features than assumed so far. Taken together, by integrating results from diagnostic classification analyses investigating groups matched for disease duration, lesion load, participant age, and gender, we identified biomarkers specific for MS patients with very early disease onset.

Conflicts of interest

The authors report no biomedical financial interests or potential conflicts of interest in the context of this work.

Source of funding

This work was supported by the Bernstein Computational Neuroscience Program of the German Federal Ministry of Education and Research (Grant Number 01GQ1001C), a clinical research group (KFO218/1) of the German Research Foundation, and the Open Access Publication Funds of the Göttingen University. The funding sources had no involvement in the study design, collection, analysis, and interpretation of data, in writing the report, and in the decision to submit the paper for publication.

Supplementary material

Supplementary material for this article can be found online at <http://dx.doi.org/10.1016/j.nicl.2014.06.015>.

References

- Banwell, B., Krupp, L., Kennedy, J., Tellier, R., Tenembaum, S., Ness, J., et al., 2007. Clinical features and viral serologies in children with multiple sclerosis: a multinational observational study. *Lancet Neurology* 6, 773–781. [http://dx.doi.org/10.1016/S1474-4422\(07\)70196-517689148](http://dx.doi.org/10.1016/S1474-4422(07)70196-517689148).
- Bakshi, R., Benedict, R.H.B., Bermel, R.A., Caruthers, S.D., Puli, S.R., Tjoa, C.W., et al., 2002. T2 hypointensity in the deep gray matter of patients with multiple sclerosis: a quantitative magnetic resonance imaging study. *Archives of Neurology* 59, 62–68. <http://dx.doi.org/10.1001/archneur.59.1.6211790232>.
- Bendfeldt, K., Klöppel, S., Nichols, T.E., Smieskova, R., Kuster, P., Traud, S., et al., 2012. Multivariate pattern classification of gray matter pathology in multiple sclerosis. *NeuroImage* 60, 400–408. <http://dx.doi.org/10.1016/j.neuroimage.2011.12.07022245259>.
- Benjamini, Y., Hochberg, Y., 1995. Controlling the false discovery rate: a practical and powerful approach to multiple testing. *Journal of the Royal Statistical Society: Series B (Statistical Methodology)* 57, 289–300.
- Bigi, S., Banwell, B., 2012. Pediatric multiple sclerosis. *Journal of Child Neurology* 27, 1378–1383. <http://dx.doi.org/10.1177/088307381245278422914372>.
- Ceccarelli, A., Filippi, M., Neema, M., Arora, A., Valsasina, P., Rocca, M.A., et al., 2009. T2 hypointensity in the deep gray matter of patients with benign multiple sclerosis. *Multiple Sclerosis (Houndmills, Basingstoke, England)* 15, 678–686. <http://dx.doi.org/10.1177/135245850910361119482861>.
- Chabas, D., Castillo-Trivino, T., Mowry, E.M., Strober, J.B., Glenn, O.A., Waubant, E., 2008. Vanishing MS T2-bright lesions before puberty: A distinct MRI phenotype? *Neurology* 71, 1090–1093. <http://dx.doi.org/10.1212/01.wnl.0000326896.66714.ae18824673>.
- Good, P., 2005. *Permutation, Parametric and Bootstrap Tests of Hypotheses* 3rd edition. Springer, New York.
- Filippi, M., Rocca, M.A., 2005. MRI evidence for multiple sclerosis as a diffuse disease of the central nervous system. *Journal of Neurology* 252 (S5), v16–v24. <http://dx.doi.org/10.1007/s00415-005-5004-516254697>.
- Ge, Y., Grossman, R.I., Babb, J.S., He, J., Mannon, L.J., 2003. Dirty-appearing White matter in multiple sclerosis: volumetric MR imaging and magnetization transfer ratio histogram analysis. *AJNR. American Journal of Neuroradiology* 24, 1935–1940. <http://dx.doi.org/10.3174/ajnr.A25213>.
- Hackmack, K., Paul, F., Weygandt, M., Allefeld, C., Haynes, J.D., The Alzheimer's Disease Neuroimaging Initiative, 2012a. Multi-scale classification of disease using structural MRI and wavelet transform. *NeuroImage* 62, 48–58. <http://dx.doi.org/10.1016/j.neuroimage.2012.05.02222609452>.
- Hackmack, K., Weygandt, M., Wuerfel, J., Pfueller, C.F., Bellmann-Strobl, J., Paul, F., Haynes, J.D., 2012b. Can we overcome the 'clinico-radiological paradox' in multiple sclerosis? *Journal of Neurology* 259, 2151–2160. <http://dx.doi.org/10.1007/s00415-012-6475-92246893>.
- Hummel, H.M., Brück, W., Dreha-Kulaczewski, S., Gärtner, J., Wuerfel, J., 2013. Pediatric onset multiple sclerosis: McDonald criteria 2010 and the contribution of spinal cord MR. *Multiple Sclerosis Journal* 0, 1–6.
- Klöppel, S., Stonnington, C.M., Chu, C., Draganski, B., Scahill, R.I., Rohrer, J.D., et al., 2008. Automatic classification of MR scans in Alzheimer's disease. *Brain: A Journal of Neurology* 131, 681–689. <http://dx.doi.org/10.1093/brain/awn31918202106>.
- Morgen, K., Sammer, G., Courtney, S.M., Wolters, T., Melchior, H., Blecker, C.R., et al., 2006. Evidence for a direct association between cortical atrophy and cognitive impairment in relapsing–remitting MS. *NeuroImage* 30, 891–898. <http://dx.doi.org/10.1016/j.neuroimage.2005.10.03216360321>.
- Polman, C.H., Reingold, S.C., Banwell, B., Clanet, M., Cohen, J.A., Filippi, M., et al., 2011. Diagnostic criteria for multiple sclerosis: 2010 revisions to the McDonald criteria. *Annals of Neurology* 69, 292–302. <http://dx.doi.org/10.1002/ana.2236621387374>.
- Prinster, A., Quarantelli, M., Orefice, G., Lanzillo, R., Brunetti, A., Mollica, C., et al., 2006. Grey matter loss in relapsing–remitting multiple sclerosis: a voxel-based morphometry study. *NeuroImage* 29, 859–867. <http://dx.doi.org/10.1016/j.neuroimage.2005.08.03416203159>.
- Renoux, C., Vukusic, S., Mikaeloff, Y., Edan, G., Clanet, M., Dubois, B., et al., 2007. Natural history of multiple sclerosis with childhood onset. *New England Journal of Medicine* 356, 2603–2613. <http://dx.doi.org/10.1056/NEJMoA06759717582070>.
- Ruggieri, M., Iannetti, P., Polizzi, A., Pavone, L., Grimaldi, L.M., 2004. Multiple sclerosis in children under 10 years of age. *Neurological Sciences: Official Journal of the Italian Neurological Society and of the Italian Society of Clinical Neurophysiology* 25 (Suppl. 4), S326–S335. <http://dx.doi.org/10.1007/s10072-004-0335-z15727227>.
- Sadaka, Y., Verhey, L.H., Shroff, M.M., Branson, H.M., Arnold, D.L., Narayanan, S., et al., Canadian Pediatric Demyelinating Disease Network, 2012. 2010 McDonald criteria for diagnosing pediatric multiple sclerosis. *Annals of Neurology* 72, 211–223. <http://dx.doi.org/10.1002/ana.2357522926854>.
- Tzourio-Mazoyer, N., Landeau, B., Papathanassiou, D., Crivello, F., Etard, O., Delcroix, N., 2002. Automated anatomical labeling of activations in SPM using a macroscopic anatomical parcellation of the MNI MRI single-subject brain. *NeuroImage* 15, 273–289. <http://dx.doi.org/10.1006/nimg.2001.097811771995>.
- Vargas-Lowy, D., Chitnis, T., 2012. Pathogenesis of pediatric multiple sclerosis. *Journal of Child Neurology* 27, 1394–1407. <http://dx.doi.org/10.1177/088307381245608422952316>.
- Weygandt, M., Hackmack, K., Pfüller, C., Bellmann-Strobl, J., Paul, F., Zipp, F., et al., 2011. MRI pattern recognition in multiple sclerosis normal-appearing brain areas. *PLoS One* 6, e21138. <http://dx.doi.org/10.1371/journal.pone.002113821695053>.
- Weygandt, M., Blecker, C.R., Schäfer, A., Hackmack, K., Haynes, J.D., Vaitl, D., et al., 2012. fMRI pattern recognition in obsessive–compulsive disorder. *NeuroImage* 60, 1186–1193. <http://dx.doi.org/10.1016/j.neuroimage.2012.01.06422281674>.
- Wilke, M., Schmithorst, V.J., Holland, S.K., 2002. Assessment of spatial normalization of whole-brain magnetic resonance images in children. *Human Brain Mapping* 17, 48–60. <http://dx.doi.org/10.1002/hbm.1005312203688>.
- Wilke, M., Schmithorst, V.J., Holland, S.K., 2003. Normative pediatric brain data for spatial normalization and segmentation differs from standard adult data. *Magnetic Resonance in Medicine: Official Journal of the Society of Magnetic Resonance in Medicine / Society of Magnetic Resonance in Medicine* 50, 749–757. <http://dx.doi.org/10.1002/mrm.1060614523961>.
- Zivadinov, R., Bergsland, N., Dolezal, O., Hussein, S., Seidl, Z., Dwyer, M.G., Vaneckova, M., Krasensky, J., Potts, J.A., Kalincik, T., Havrdová, E., Horáková, D., 2013. Evolution of cortical and thalamus atrophy and disability progression in early relapsing–remitting MS during 5 years. *AJNR. American Journal of Neuroradiology* 34 (10), 1931–1939. <http://dx.doi.org/10.3174/ajnr.A350323578679>.